CHAPTER 5

Geologic Interpretation of DIGHEM^{IV} Airborne Aeromagnetic and Electromagnetic Data over Unga Island, Alaska

By John W. Cady and Bruce D. Smith

U.S. GEOLOGICAL SURVEY OPEN-FILE REPORT 99-136

Geological and Geophysical Setting of the Gold-Silver Vein Systems of Unga Island, Southwestern Alaska

CONTENTS

Figures

Geologic Interpretation of DIGHEM^{IV} Airborne Aeromagnetic and Electromagnetic Data over Unga Island, Alaska

John W. Cady and Bruce D. Smith

INTRODUCTION TO THE AIRBORNE GEOPHYSICAL SURVEY

A DIGHEM^{IV}* airborne electromagnetic (EM) and magnetic survey was flown in 1990 by DIGHEM, Inc. over 105 km^2 of southeastern Unga island (fig. 1) for Battle Mountain Gold Company (hereafter, BMGC), which was conducting minerals exploration for the Aleut Corporation of Anchorage. The Aleut Corporation has granted permission to USGS and BMGC to include here the results of the airborne survey. The geophysical data were previously interpreted by the contractor (Pritchard, 1990) for purposes of identifying EM anomalies in terms of possible sulfide deposits, conductive overburden, or bedrock structures; EM anomalies were prioritized for ground follow-up. Our objective in including the data here is to specifically aid in the new geologic and structural interpretations that are discussed by Riehle and others (Chapter 2) and by Riehle (Chapter 4) by providing control in areas of overburden and by constraining extrapolation of surface observations to depth.

In this chapter, we briefly explain collection and analysis of the data, and make qualitative interpretations of the data to characterize the geophysical setting of the mineralized trends and map lithologic and structural features on the surface and in the subsurface. We explore the relationships between gridded apparent resistivity, discrete bedrock conductors, aeromagnetics, topography, mapped geology, and air photo lineaments using modern tools of geophysical analysis and image processing. We use the geophysical data primarily as a geologic mapping tool, and in some case we make hypotheses that can be tested by fieldwork. The next step should be to take the geophysical data and their interpretation to the field to test the hypotheses made in this report.

The objectives of this USGS geophysical study were to use the data from Unga Island to characterize the geophysical setting of the known gold deposits and to assist mapping structural and lithologic features on the surface and especially in the subsurface. The USGS funded DIGHEM to retrieve the digital geophysical data and do minor reprocessing to improve the apparent resistivity data described in the following sections. No additional processing or interpretation of the data from Popof Island was done for this project. The digital data from DIGHEM included grids of the electromagnetic data (apparent resistivities at 900, 7200, and 56000 Hertz and VLF) and total magnetic intensity. These grids were imported into ER Mapper* software for additional processing and plotting. All of the digital data from DIGHEM, as well as the contractor's report and grids and algorithms in ER Mapper format, are included in the Geophysics folder on the CD-ROM publication.

---

* Product names are for descriptive purposes only and do not imply endorsement by the U.S. Geological Survey.

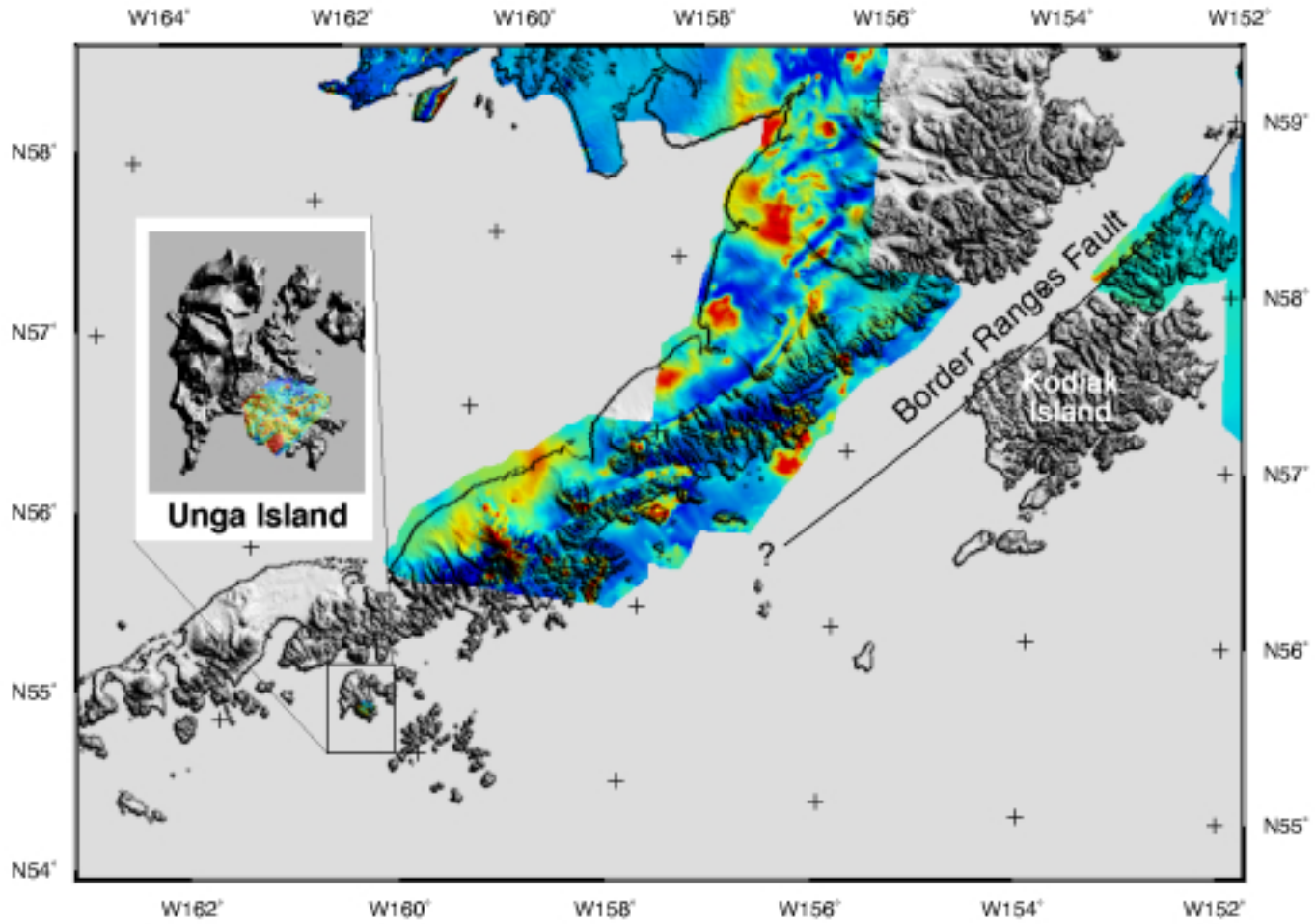

Figure 1

Figure 1. Location of the Unga Island survey. Available regional magnetic data in color are from a 1 km grid (Saltus and Simmons, 1997) overlain on digital topography (grey-shaded relief). Detailed aeromagnetic data discussed below.

REGIONAL GEOPHYSICAL SETTING OF UNGA ISLAND

The survey area is isolated from regional aeromagnetic data by about 85 km (fig. 1), so the interpretation of these data lacks a regional geophysical context. To anticipate the results of our interpretation: magnetic and EM anomalies in the airborne survey of southeastern Unga Island are caused almost entirely by lithologic variations within the Popof volcanic rocks described by Riehle and others (Chapter 2). These variations are the result both of primary lithologic contacts and secondary alteration. Riehle and others (Chapter 2, fig. 1) summarize the evidence for the location of the Border Ranges fault, which from Kodiak Island to the northeast separates the Peninsular terrane (part of the Wrangellia composite terrane of Plafker and others, 1994) from the Chugach terrane. The fault can be traced for most of its 1000-km length by magnetic anomalies caused by Jurassic mafic plutonic rocks and lesser ultramafic rocks of the Peninsular terrane. The trace of the Border Ranges Fault (BRf) on Figure 1 was mapped by Fisher (1981) using limited marine (not shown) and airborne magnetic data. However, in the vicinity of the Shumagin Islands, there is no regional magnetic evidence as to the location of the BRf.

If the BRf passes between the outer and inner Shumagin islands (south of Unga Island), then it is possible that the magnetic rocks on Unga Island belong to a northeast-trending suite of magnetic Tertiary volcanic rocks (B3 and C3 of Moll-Stallcup and others, 1994) that cause magnetic highs to the northeast along the southeastern shore of the Alaska Peninsula. However, Saltus and others (in press) use ship magnetic data west of the Alaska Peninsula to suggest that the Wrangellia composite terrane and Chugach terranes of Plafker and others (1994) cross the Alaska Peninsula. They imply that the BRf runs east west across the peninsula south of Lat. 56° N. They show Unga Island lying within the Chugach Terrane, an interpretation that would suggest that the magnetic highs on Unga Island correlate with magnetic highs caused by sources beneath the Bering Sea. In the absence of more complete magnetic coverage, this controversy remains unresolved.

In the remainder of this chapter, we discuss detailed interpretations of the aeromagnetic and EM data without regard to their regional setting.

GEOPHYSICAL EXPRESSION OF EPITHERMAL-GOLD DEPOSIT MODELS

Wilson and others (1996) adapted mineral deposit models from Cox and Singer (1986) in order to make a quantitative mineral resource assessment of the Port Moller quadrangle. They developed a composite epithermal gold model for the Shumagin, Apollo, and Sitka deposits based upon the Creede epithermal gold model, the Hot Springs gold-silver model, and the Sado-type gold model. Singer (Chapter 7) concludes that the Sado deposit type best fits the Shumagin and Apollo systems. Features of possible geophysical significance in the Shumagin deposit include a pyrite-rich cataclasite and minor sulfides in quartz-breccia veins. In the Apollo deposit, calcite-bearing open-growth quartz veins contain ore consisting of free gold, pyrite, galena, sphalerite, chalcopyrite, and native copper. The Sitka deposit has sulfide-bearing open-growth quartz veins that contain as much as 5 percent chalcopyrite, galena, and lesser sphalerite.

Klein and Bankey (1992) compiled a geophysical model of Creede, Comstock, Sado, Goldfield and related epithermal precious metal deposits. Pertinent characteristics of this model are 1) The geologic setting includes faulted, fractured, and brecciated andesitic to

rhyolitic lavas and tuffs, hypabyssal, porphyritic dacite to quartz monzonite intrusions. 2) Deposits occur in the edifice of volcanic morphologic features, often near edge of a volcanic center, or above or peripheral to intrusions. 3) Deposits are commonly associated with resurgent caldera structural boundaries. 4) Short-wavelength magnetic anomalies are common over volcanic terranes because of variable magnetizations and polarizations. This pattern may contrast with an area of moderate to intense alteration that will display a longer-wavelength low, often linear in the case of vein systems, caused by destruction of magnetite (e.g. lineament ML2 on figs. 3 and 4 of this chapter). Local magnetic highs may be associated with hypabyssal intrusions. 6) Regional resistivity is generally low for weathered and altered andesitic to rhyolitic volcanic rocks as compared to high resistivity typical of buried intrusions. 7) Magnetic lows will be associated with alteration; however, discriminating such lows from the background may be difficult on a deposit scale. 8) A resistivity high flanked by resistivity lows is characteristic of a simple and idealized quartz-adularia vein system with associated argillic to propylitic alteration. However, there may be geologic structures and petrologic complications that distort this ideal picture. More generally, resistivity lows will be associated with: 1) Sulfides when concentrated and connected at about 5-percent volume or more, 3) argillic alteration, and 3) increased porosity related to wet, open fractures and brecciation. Resistivity highs will be associated with zones of silicification, intrusion, or basement uplifts.

PREVIOUS INTERPRETATIONS OF UNGA ISLAND GEOPHYSICAL DATA

Ellis and Apel (1991) and Ellis (1992) report geologic fieldwork done by BMGC to follow-up the detailed airborne geophysical survey described in this report. Ellis and Apel (1991, p. 12-13) report that "Generally, tuffs are more intensely altered than adjacent flows and lithic tuffs are typically more pyritic than crystal tuffs." They describe a sequence of alteration increasing from propylitic through several stages of argillic alteration to pervasive argillic, which is characterized by complete clay alteration. Pyrite mineralization in pervasive argillic "...is greater than 5% and may occur as zones of massive sulfide replacement." They also found (p. 17) that "...faults on Orange Mountain are mostly minor, northeast trending, east dipping, adjustment structures. One major fault trends N30W and dips 62 degrees SW. The intersection of the major fault with the northeast-trending faults provides good ground preparation for ore deposition. The N30W fault could be a conduit through which the mineralizing fluids moved."

In describing the results of the EM survey, Ellis and Apel (1991, p. 13-15) identify a Zone 1 anomaly, located in a largely brush covered area between Orange Mountain and Prays (fig. 2). They state that "...The cause of the Zone 1 resistivity low is not certain; however, it is thought to be at least in part due to previously undetected clay and pyrite alteration of tuffs which are correlative with Orange Mountain tuffs. The Zone 1 anomaly coincides with a triple intersection of NW and NNE trending mapped faults and satellite linears and the NE trending Shumagin Mineral Trend. Conductive trends within the resistivity low parallel these NE and NNE structural trends." They also identify a Zone 2 anomaly located approximately 2 miles northeast of the Apollo Mine. "...It has no known mineralization, alteration, or anomalous geochemistry associated with it, but because of its location on the Apollo trend and its geophysical signature, further investigation is warranted" (Ellis and Apel, 1991, p. 15)

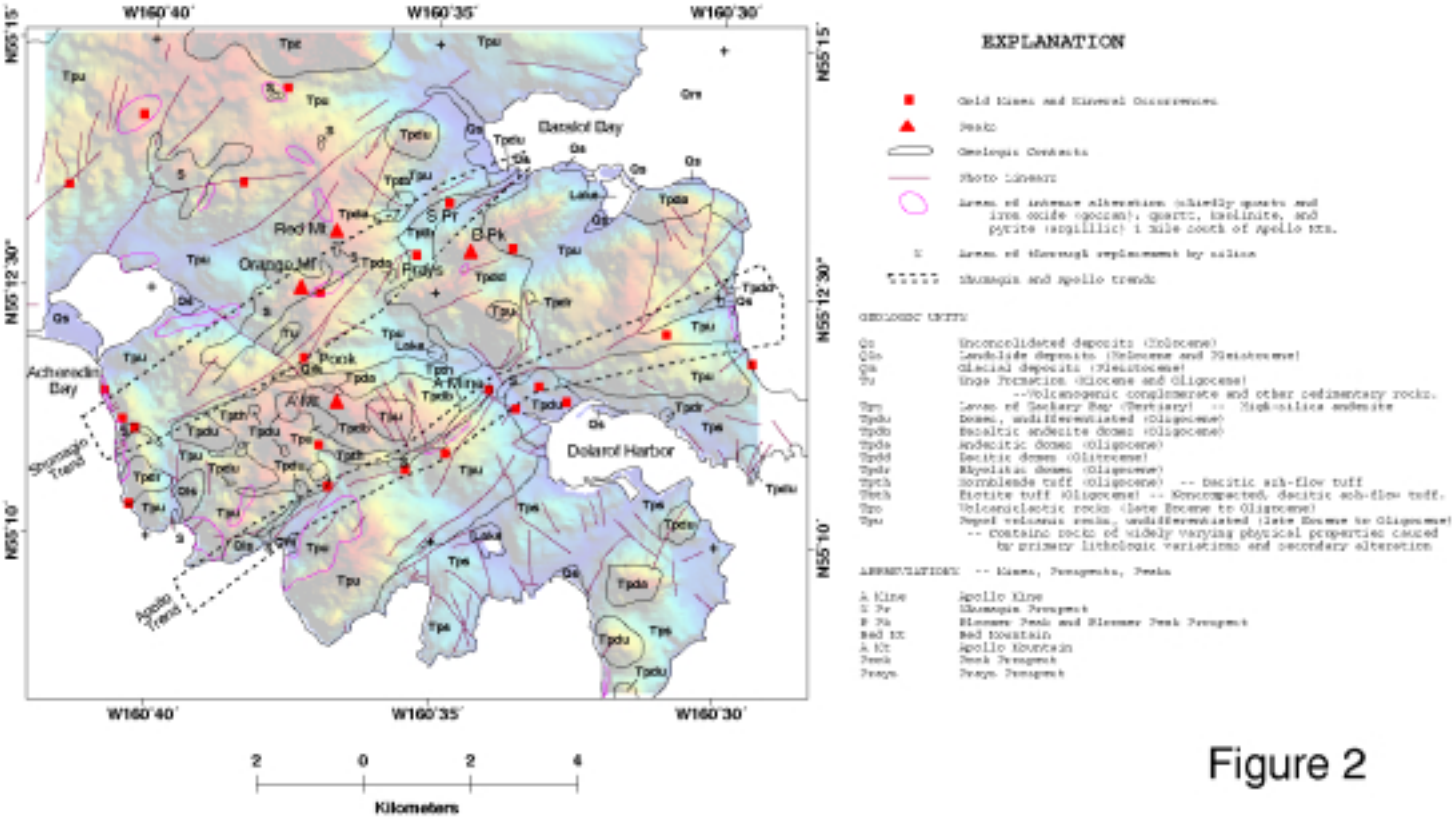

Figure 2

Figure 2. Geologic overlay of Unga Island, with unit symbols and brief unit descriptions, modified from Riehle and others (Chapter 2). Gold mines and mineral occurrences from Wilson and others (1996). Line information used as overlay in subsequent figures. Overlain on topography illuminated from the northeast. Topography in this and Figures 4-9 are from 1:63,360 topographic maps digitized by line-following at a 30-m interval and regridded at 16.67 m for the figures.

Ellis (1992, p. 11) described the Orange Mountain Resistivity Low (OMRL) thus: "...Widespread and locally intense hydrothermal alteration has affected the andesitic and basaltic rocks in the OMRL area and produced a spectacular 2.7 square mile color anomaly. Silicification is most intense and is centered at Orange Mountain and, to a lessor extent, at the Pray's and Pook prospects. Strong to pervasive (typically pyritic) argillic alteration extends up to two miles south and east from Orange Mountain. A well-defined airborne resistivity low delineated the pyritic, argillically altered rocks within the OMRL, and a moderate resistivity high is centered over Orange Mountain silicification." The OMRL is the conductive triangle between Orange Mountain, the Apollo Mine, and Apollo Mountain in our maps of apparent resistivity (figs. 5-7). Ellis attributes the OMRL to argillic alteration, and also refers to *structurally controlled* gold targets within the OMRL (italics added).

Ellis (1992, p. 9-10) extrapolated from high-grade adularia-sericite veins to large disseminated deposits: "...Over 30 gold prospects occur on Unga Island. The vast majority of these are narrow gold bearing epithermal veins and faults that lie within either the Apollo or Shumagin trends_ A number of these gold showings have the potential to develop additional vein ore chutes; however, vast areas of strongly altered, structurally prepared, permeable volcanics could host larger disseminated gold deposits_" The most significant cluster of gold anomalies (>25 ppb) occurs at Pook where 60 BMGC soil, rock, and auger samples were found within a 2500' long by up to 1000' wide area. The majority of these anomalies were low level (80% <100 ppb) with only high-graded vein samples approaching "ore grade" (0.13 oz/t Au).

Our data processing and initial interpretation, done independently of that by Ellis, confirmed his identification of Zones 1 and 2, the OMRL, and the intersection of northeast-trending mineralized trends, north-northeast trending lineaments, and northwest-trending faults. Having no opportunity to go to the field on Unga Island, we were plagued by the question, "What is the significance of the large triangular area of low resistivity overlying undifferentiated Popof volcanic rocks (unit Tpu) south of Orange Mountain and hornblende tuff (unit Tpth) north of Apollo Mountain and the Apollo Mine?" Ellis correlated among that resistivity low, a 6.9 km^2 (2.7 mi^2) color anomaly caused by argillic alteration, and elevated gold chemistry. He attributed the OMRL to argillic alteration of volcanic rocks, some of which are tuffs, although, as Ellis and Apel (1991, p. 15) admit, "since alteration is so intense, most of the original rock types cannot be identified with any certainty except for a propylitically altered andesite flow." Geologic mapping at inch-to-the-mile scale (Riehle and others, Chapter 2) shows no mapped tuffs in the immediate vicinity of Orange Mountain, although small amounts of tuff occur locally within unit Tpu (J. Riehle, written commun., 1998). Conversely, areas of mapped, altered tuffs elsewhere on Unga Island (such as south and west of Apollo Mountain) generally correlate poorly with resistivity lows; moreover, neither Riehle and others (Chapter 2) nor Ellis and Apel (1991) infer that tuffs are a dominant lithology at the Zone 2 geophysical anomaly, northeast of the Apollo mine.

Ellis (1992) further hypothesized that the OMRL may contain large deposits of disseminated gold. We defer to Ellis on this interpretation.

UNGA ISLAND GEOPHYSICAL DATA

Total survey coverage for Unga and Popof islands was 820 line kilometers. Data and interpretations that follow are for the Unga Island survey (fig. 1, inset), which covers an area

approximately 8 km by 12 km on the southeastern peninsula of Unga Island (Pritchard, 1990).

The survey over Unga Island was flown by helicopter along flight lines running northwest and southeast (315° and 135°), with nominal line spacing of 152 meters and an average airspeed of 70 km/hr. The geophysical data were recorded 10 times per second, yielding an average sample interval along the flight lines of 2 m. The nominal height of the EM "bird" was 30 meters above terrain, although in areas of rough terrain, bird height sometimes exceeded 100 m. Electromagnetic data were collected at 900 Hz, 7200 Hz, and 56000 Hz. Magnetic data were collected with a Cesium vapor magnetometer towed between the EM bird and the helicopter, nominally 45 m above terrain. The VLF receiver was towed between the magnetometer and the helicopter, nominally 50 m above terrain. Navigation and position recovery used a UHF electronic positioning system and a video-tracking camera.

Processing by DIGHEM produced paper maps and digital gridded data. DIGHEM provided digital flight line data as well, which we used to examine selected anomalies, but we did not systematically process or interpret these data. We used the following grids, which had a square cell size of 16.67 m x 16.67 m:

1. Apparent resistivity in ohm-m at 900 Hz. These data were clipped by DIGHEM to show a maximum apparent resistivity of 1035 ohm-m, which is the limit of system sensitivity at this frequency.
2. Apparent resistivity in ohm-m at 7200 Hz.
3. Apparent resistivity in ohm-m at 56000 Hz.
4. Total magnetic intensity in nT.
5. In addition to the digital grids, we digitized a paper map showing 1022 anomalous electromagnetic (EM) responses identified using a near-vertical, half-plane model. These were categorized by DIGHEM as discrete bedrock conductors (735), conductive cover (276), rock unit or thick cover (10), and edge of wide conductor (1). Only the discrete bedrock conductors are displayed (as small black squares) in the geophysical figures that follow.

Grids of the VLF data were plotted and analyzed in conjunction with the other data, but the VLF data were noisy, did not appear to be significant to the geologic interpretation, and are not reported herein.

Unit contacts and other line information from the geologic map (Riehle and others, Chapter 2) are included for reference in the figures of geophysical data that follow. The lines alone, overlain on topography, are shown in Figure 2 because some of the lines are not clearly visible on the maps of raster data.

GEOLOGIC INTERPRETATION OF AEROMAGNETIC DATA

Introduction

Aeromagnetic surveying exploits variations in the percentage of magnetic minerals, primarily magnetite, in common rocks. Volcanic rocks tend to be magnetic, and sedimentary rocks nonmagnetic. However, since the aeromagnetic survey was almost entirely over volcanic rocks, the variations of interest result from variations in the magnetite content of the volcanic rocks and are assumed to be caused by 1) primary variations in composition of the volcanic rocks, and 2) secondary alteration, which at low metamorphic grades tends to

destroy magnetite and cause magnetic lows. The primary use of aeromagnetic data on Unga Island is geologic mapping, including the mapping of alteration. Pyrrhotite is a weakly magnetic mineral that can be detected by the aeromagnetic method, permitting direct magnetic detection of massive sulfides. However, there is no correlation between magnetic anomalies and mineralized trends in the Unga Island survey, so direct detection of massive sulfides does not appear to be possible here.

We processed the aeromagnetic grid to reduce it to the north magnetic pole, a process that causes magnetic anomaly highs to be centered over the causative bodies and gradients to occur over boundaries between magnetically different units. The process assumes that all magnetization is induced parallel to the Earth's magnetic field, with an inclination of 67.8 degrees and a declination of 17.3 degrees, and calculates a new grid with a vertical inclination. The effect of reduction to the pole (RTP) on Unga Island is to shift positive magnetic anomalies approximately 100 m north-northeast, which is significant relative to the flight line spacing of 152 m.

The RTP magnetic map (fig. 3A, also shown without vector overlays as fig. 3B) shows a complex pattern of magnetic highs (red) scattered against a background of lower magnetic intensity (blue) that represent the local absence of magnetic rocks. Areas of magnetic highs are underlain chiefly by undifferentiated Popof volcanic rocks (unit Tpu). Areas of magnetic lows are inferred to be associated with nonmagnetic volcanic rocks or, in the southernmost part of the survey, sedimentary rocks. Areas of intermediate magnetic intensity (yellow and green) are extensions of the areas of high magnetic intensity and are interpreted to be caused by thinner and (or) more deeply buried magnetic units, probably flows. Structural information is evident in the aeromagnetic data, but it is shown by features that are secondary to the overall scatter of magnetic highs.

Interpretation of Magnetic Anomalies

A large part of the map averages about 52,000 nT, has typical magnetic relief of 50 to 200 nT, and is portrayed in green and yellow. This is the background over most of the volcanic terrain, against which the anomalies are observed, and is probably caused by weakly magnetic volcanic rocks. Magnetic anomaly highs ("magnetic highs"), shown mainly in red, include the following types:

1. Intense subcircular anomalies 100 to 700 m in diameter, with amplitudes of 1000-1500 nT. (Labeled A, B, D1-D2, E1-E4, F1-F7, and G1-G22).
2. Irregular curvilinear belts of anomalies, many of which are comprised of strings of subcircular anomalies. Typical amplitudes are 500-800 nT. (E1-E4, F1-F7, G1-G5, C1-C8, etc.)
3. In the southernmost part of the map, is a 2x3-km area defined by a magnetic high with amplitude ranging from 400 to 2700 nT. Peaks of this high, labeled K1-K4, may be coalescence of magnetic highs of type 1.

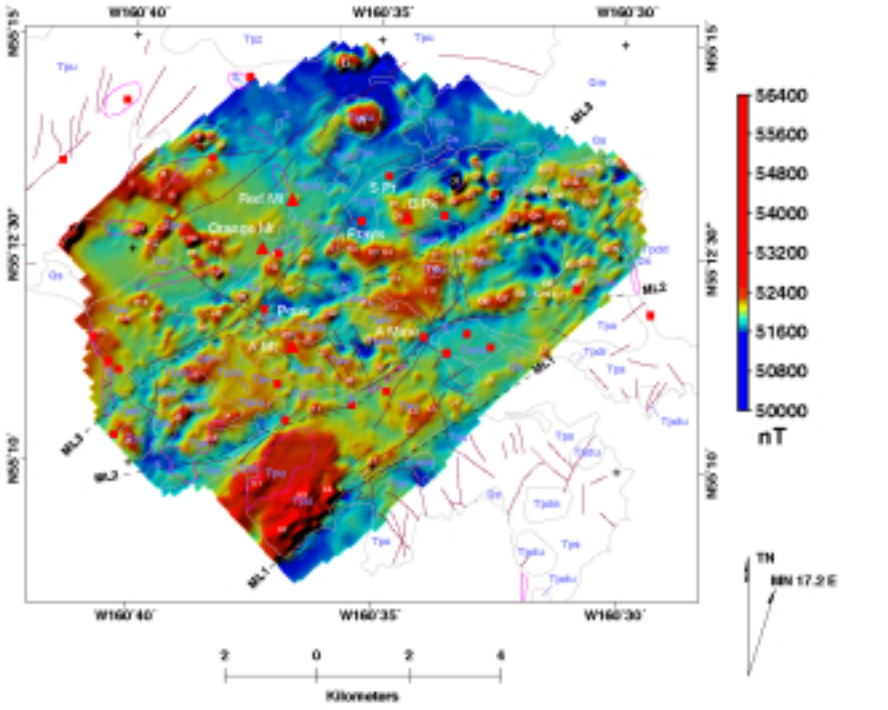

Figure 3A

Figure 3A. Total magnetic intensity reduced to the north magnetic pole. Magnetic intensity displayed in shaded relief with illumination from the northwest to emphasize northeast-trending magnetic discontinuities identified by dashed lines ML1, ML2, and ML3. Geologic overlay described in Figure 2.

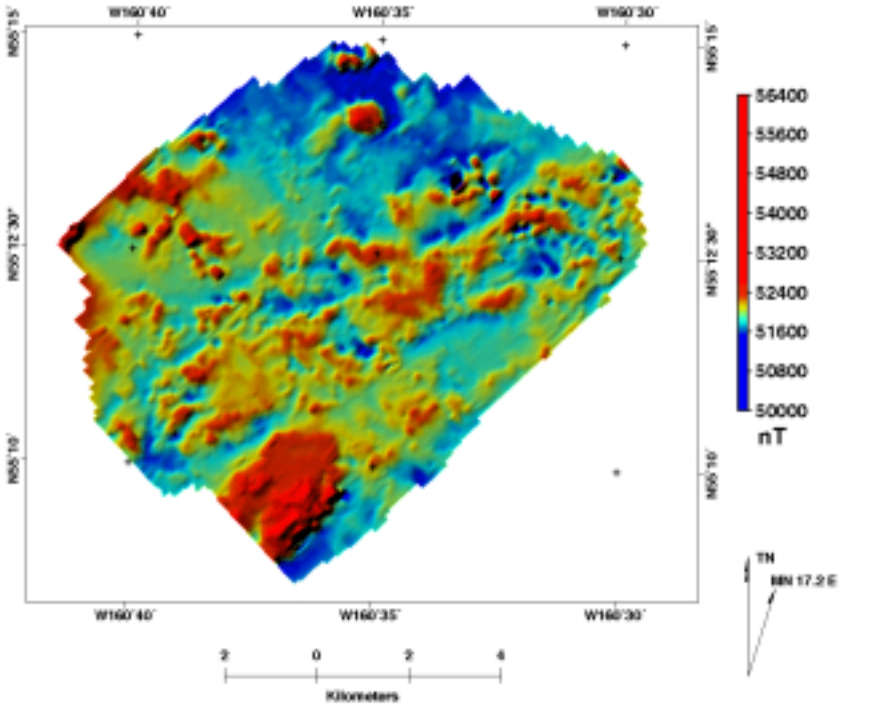

Figure 3B

Figure 3B. Total magnetic intensity reduced to the north magnetic pole. Same as Figure 3A, but geologic overlay omitted.

4. We interpret the magnetic highs to be caused by undifferentiated Popof volcanic rocks (unit Tpu). The largest, best-defined subcircular anomaly (A) is caused by a mapped dome of unit Tpdu (see also fig. 4). Based upon this excellent example, we infer that most of the anomalies of type 1 are caused by mapped and unmapped domes. A good candidate for an unmapped dome is anomaly B. Other anomalies associated with mapped dome rocks include E1, G18, and J5 (Tpda), and J3 (Tpdu). Some domes do not have associated subcircular highs, however, and many small sbcircular highs occur in areas of undifferentiated Popof volcanic rocks (Tpu). If the smallest intense highs are caused by domes, the domes are very small, only 100 m in diameter.

A simple estimate of the distance from the airborne magnetometer to the top of a magnetic source is the width of the steepest magnetic gradient bounding a magnetic anomaly. Measurements of characteristic anomalies on the map show that most of the anomaly sources have tops at or near the surface. Because porous rocks are more susceptible to magnetite-destroying alteration than hard, crystalline rocks, we hypothesize that the domes are the most magnetic, then the flows, with the least magnetic rocks being tuff and flow breccia. Magnetic highs occurring in areas mapped as undifferentiated Popof volcanic rocks (Tpu) probably indicate lava flows and unmapped domes, some of which may have a thin cover of less-magnetic tuff and flow breccia. The best way to test these interpretations is by detailed geologic field work using a magnetic susceptibility meter.

South of Baralof Bay is an aggregation of intense magnetic highs of the type attributed to domes (C1-C7 in unit Tpu and D1-D2 in unit Tpdd). The highs occur on the northeast trending ridge (figs. 2 and 4) that includes Bloomer Peak. The ridge is surrounded by a magnetic low and arcuate geologic boundaries that suggest that the ridge and the magnetic anomalies could be caused by an ovoid igneous feature. The Shumagin prospect (SPr) lies on the northwest margin of the arcuate feature. It is tantalizing to speculate that a small caldera might be responsible for the arcuate features, but such an interpretation should be based upon geologic mapping rather than a very tenuous geophysical interpretation.

Within the aggregation of magnetic highs are two very anomalous magnetic features labeled C4 and C8. C4 is an intense magnetic high (86,029 nT in the total magnetic intensity profile data) and C8 is an intense magnetic low (29,040 nT in the total magnetic intensity profile data). These intensities deviate from background (52,000 nT) by tens of thousands of nT, extremely rare for geological sources but typical of magnetite iron ore deposits (e.g. Gunn and Dentith, 1997). Each of these anomalies occurs on a single profile in the raw data. We are suspicious that they the result of either cultural features or a transient electromagnetic phenomenon in the atmosphere, because both coincide with anomalies in the "spherics" and "powerline" monitor channels of the Dighem system. However, other similar anomalies in the monitor channels, which occur on fewer than 25 flight lines in the northeastern part of the survey, are not accompanied by magnetic anomalies. Cultural features (steel structures, powerlines) are extremely unlikely in this remote location. A surface magnetometer profile across each could be used to check the reality of these anomalies. Incidentally, Ellis (1992) reports a 4000 nT magnetic low and a coincident gold-arsenic geochemical anomaly at Red Cove prospect on Popof Island.

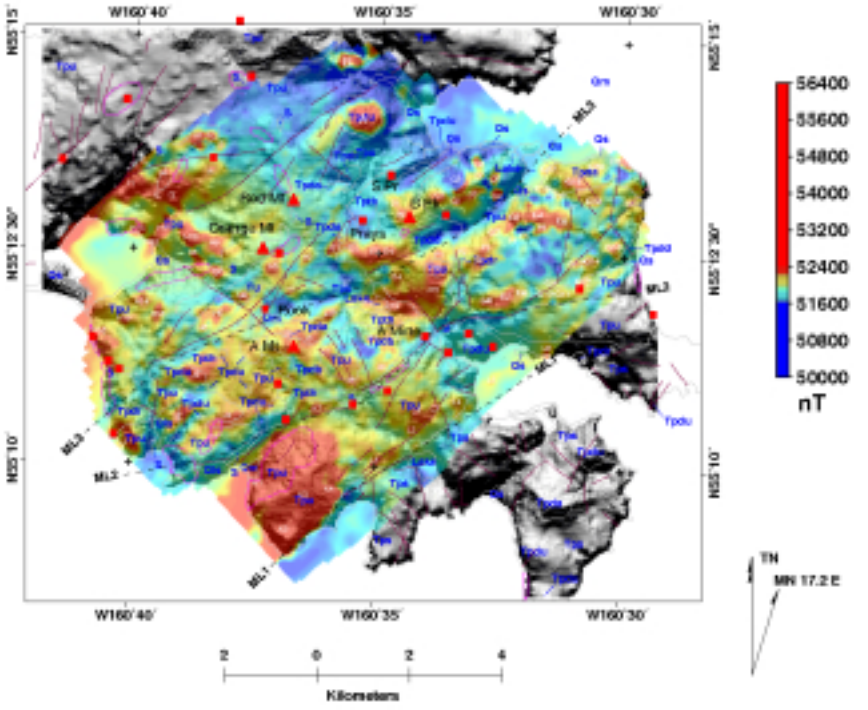

Figure 4

Figure 4. Total magnetic intensity reduced to the north magnetic pole (color), superimposed on topography (grey-shaded relief illuminated from the northeast. Topographic data are from 1:250,000 scale digital elevations models having a grid spacing of 6 arc seconds in longitude and 3 arc seconds in latitude, regridded to square 16.67x16.67 m cells. The letters indicate magnetic anomalies described in text. Geologic vector overlay described in caption for Figure 2. Magnetic discontinuities ML1-ML3 discussed in text.

Magnetic anomalies must be interpreted together with topography for two reasons: 1) Although the survey was designed for constant ground clearance, the aircraft may fly low and close to magnetic sources over ridges, high and further from magnetic sources over valleys. This can cause false magnetic highs over ridges and lows over valleys. 2) Magnetic properties and resistance to erosion are both a function of lithology, resulting to a correlation (either positive or negative) between the magnetic and topographic maps. In this case, the magnetic anomalies are real, and their correlation with topography can be exploited in the geologic interpretation.

Figure 4 shows the magnetic data in color superimposed upon topography illuminated from the north. Correlative magnetic and topographic highs are scattered across the map. The best examples are anomalies A and B, where magnetic highs coincide with topographic peaks attributed to mapped (A) and unmapped (B) domes.

In the southern apex of the aeromagnetic map is a 2x3-km zone of magnetic highs (e.g. K1-K4) with amplitudes ranging from 400 to 2,700 nT. The area of high magnetic intensity coincides overall with a broad northeast-trending topographic ridge mapped as undifferentiated Popof volcanic rocks (Tpu). The zone of magnetic highs is asymmetric, with the main peaks (K2-K4) occurring south of the topographic ridge. High resistivity occurs on the northwestern flank of the ridge, roughly coincident with a large area of silicic alteration. The magnetic anomalies over this ridge are different in character from other anomalies on the map, in that they have high intensity over a wider area than anomaly types 1-3. They probably represent a strong coalescence of anomalies caused by domes and flows, but it is possible that they are caused instead by a buried pluton.

In contrast to magnetic anomaly types 1-4 are magnetic lows shown in blue, with magnetic intensity of 51,600 nT or less. There is a curious decrease in magnetic intensity towards the north, seen as a blue area of low relief surrounding magnetic high A. The low occurs mainly over undifferentiated Popof volcanic rocks (Tpu), which are commonly magnetic elsewhere. Is the magnetic low the effect of alteration of the Popof volcanic rocks, perhaps in a broad metamorphic aureole surrounding the dome at A? Or is the low caused by a thinning to the north of Popof volcanic rocks over non-magnetic sedimentary rocks of the Unga Formation (Tu)? The magnetic map covers too small an area to determine the regional magnetic setting, but the answer should be obvious in a regional magnetic map.

We identified three curvilinear belts (lineaments) characterized by magnetic lows labeled ML1-ML3 in Figures 3 and 4. ML1 separates magnetic highs over undifferentiated Popof volcanic rocks (Tpu) to the north from an area of low magnetic relief over volcaniclastic rocks (Tps) to the south. As the aeromagnetic map terminates less than 1 km south of the lineament, we do not know whether the lineament is regionally significant. Lineaments ML2 and ML3 are defined by discontinuous magnetic lows 100 to 300 m wide that separate regions of higher magnetic relief. A commonly given, rarely proven cause for such magnetic lineaments is destruction of magnetite by alteration along shear zones (c.f. Klein and Bankey (1992), cited above).

The magnetic lineaments commonly coincide with valleys or breaks in topography (fig. 4), features that are often associated with shear zones. The valleys may also contain nonmagnetic sediments that would contribute to the magnetic lows. Lineament ML2 corresponds (except at its poorly defined southwestern end) to the silicified Apollo trend containing the Apollo mine and other mines and prospects. Lineament ML3 has not been identified in the geology,

although it is 100 to 200 m south of mapped photo lineaments along a third of its length. It is everywhere south of the Shumagin trend (fig. 2).

The similarity of magnetic terranes to either side of ML2 and ML3 suggest that they have no great offset, either vertical or horizontal. For example, an alignment of type 2 magnetic highs (E1-E4) north of ML3 appears to line up with a similar alignment (F1-F7) south of ML3). Several domes are mapped between lineaments ML2 and ML3, suggesting that the intervening block has been uplifted and eroded a small amount--perhaps equivalent to the thickness of tuffaceous cover--at most a few hundred meters. Lineament ML3 forms the southern boundary of the aggregation of magnetic anomalies labeled C1-C8 and D1-D2.

Aside from anomaly C8, which may be the result of a data error, there are no obvious magnetic lows caused by reverse remanent magnetization. The best candidates are the complex magnetic lows between highs labeled F5, G9, and G13, and a low south of high J11 near the Apollo Mine. However, as these magnetic lows coincide with topographic lows, they are most likely the result of nonmagnetic, easily eroded rocks. Field work with a magnetic susceptibility meter or a magnetometer could resolve the issue.

GEOLOGIC INTERPRETATION OF AIRBORNE ELECTROMAGNETIC DATA

Introduction

Electromagnetic (EM) prospecting exploits variations in conductivity (or its inverse, resistivity) that occur in mineralized rocks. For example, argillic alteration forms wide areas of moderate conductivity, and connected veins of massive sulfide are highly conductive (Klein and Bankey, 1992). In contrast, silicic alteration may form areas of high resistivity.

Figures 5, 6, and 7 display apparent resistivity ($\tilde{n}_a$ in ohm-m calculated at 900 Hz, 7200 Hz, and 56000 Hz respectively, herein called "resistivity" for brevity). Blues show resistivity highs, reds resistivity lows (conductivity highs). Topography is displayed in the background as grey-shaded relief, illuminated from the northeast. Resistivity data is masked out over seawater, which is conductive at all three frequencies.

The overall distribution of resistivity is qualitatively the same at all frequencies. Somewhat more spatial detail is shown at 56000 Hz, which responds to near-surface conductors, whereas resistivity calculated for the lower frequencies, which penetrate deeper, vary more smoothly. The resistivity z-scales of Figures 5-7 shows that the total range of resistivity is greatest at 56000 Hz, and diminishes at lower frequencies. Maximum resistivity at 900 Hz is unknown, for the data were clipped at 1035 ohm-m.

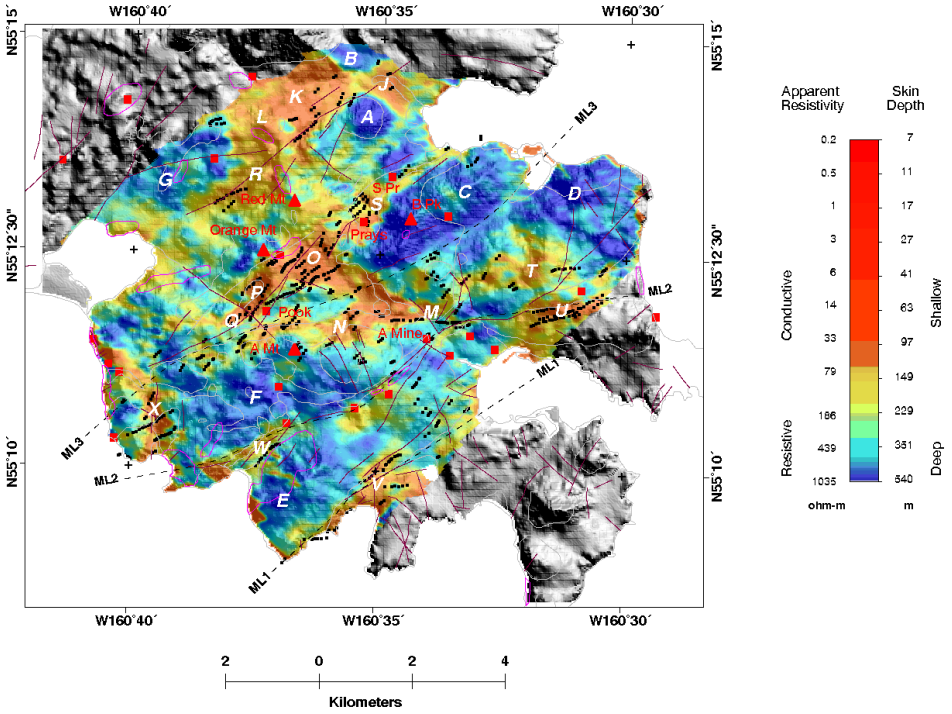

Figure 5

Figure 5. Apparent resistivity at 900 Hz, superimposed on topography in shaded relief illuminated from the northeast. Italicized letters indicate features discussed in text. Square black spots indicate "discrete bedrock conductors", probably sulfide or clay in veins and faults, digitized from the DIGHEM report (Pritchard, 1990).

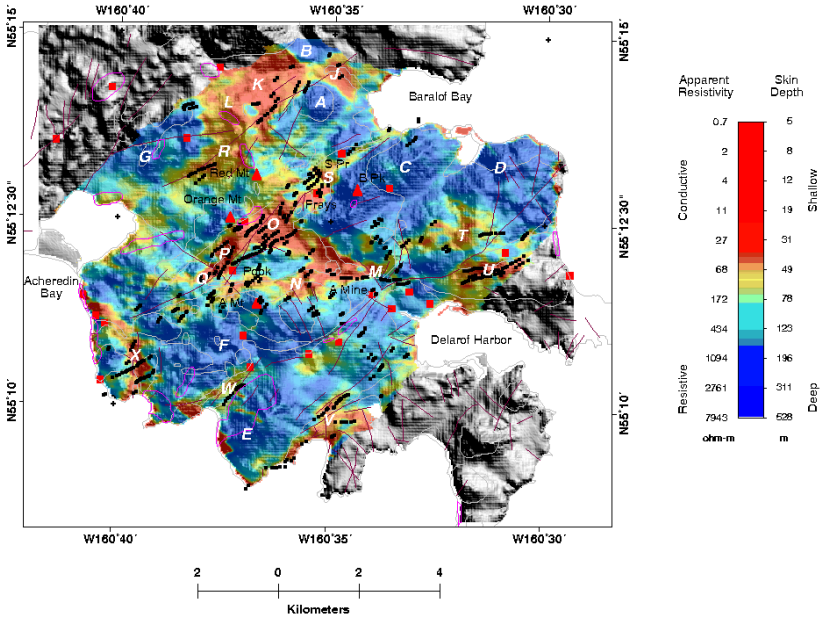

Figure 6

Figure 6. Apparent resistivity at 7200 Hz, superimposed on topography in shaded relief illuminated from the northeast. Italicized letters indicate features discussed in text. Square black spots indicate "discrete bedrock conductors".

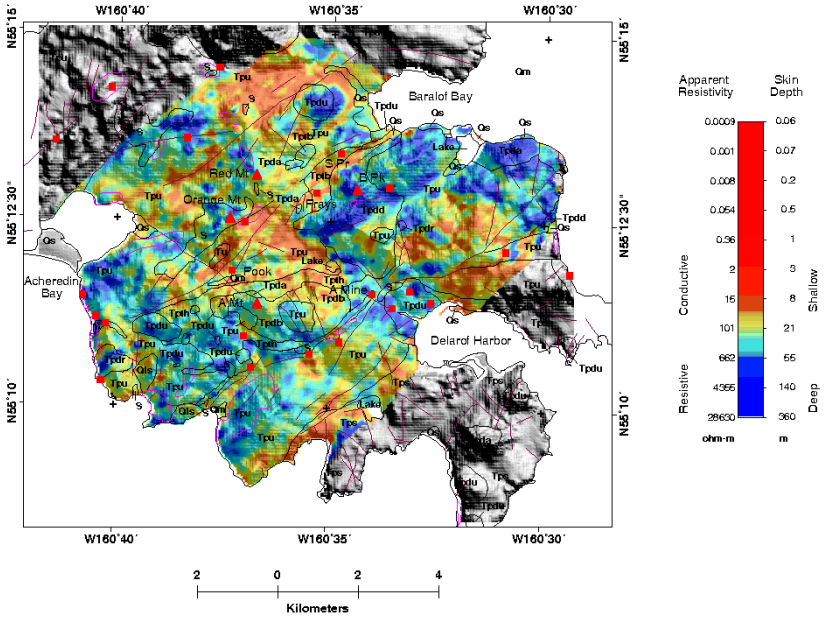

Figure 7

Figure 7. Apparent resistivity at 56,000 Hz, superimposed on topography in shaded relief illuminated from the northeast. Italicized letters indicate features discussed in text. Bedrock conductors shown in Figures 5 and 6 are eliminated to avoid obscuring details of the resistivity map.

A measure of how deep EM systems can penetrate is given by the skin depth, δ, in meters. This is the depth at which the amplitude of a plane wave signal has dropped to 37 percent of its original value.

$$\delta = 503 (\rho_a / f)^{1/2}$$

where r_a is the apparent resistivity and f is the operating frequency of the system in Hz. Skin depth is displayed on Figures 5,6, and 7 by the expedient of adding skin depth to the z-scale. To anticipate the analysis that follows, the significance of skin depth to the present study is this: Known mineralization tends to be in the more conductive areas, or at the boundary between conductive and nonconductive areas. The z-scales are chosen such that the green-blue transition separates conductive from nonconductive areas. Maximum depths of penetration in conductive areas are approximately 50 m at 56000 Hz, 100 m at 7200 Hz, and 350 m at 900 Hz, and the bedrock conductors occur in areas with a skin depth of 50 m or less at 7200 Hz. Therefore, any exploration targets associated with conductive rocks, especially at the higher frequencies, are shallow.

In addition to calculating apparent resistivity, DIGHEM calculated the properties of 1022 anomalous EM responses, and determined that 735 of these were discrete bedrock conductors (i.e. those attributable to sulfide or clay in veins and faults, as opposed to conductive overburden or thick cover-rock units). The model used to identify conductors best reflects discrete bedrock conductors (hereafter called simply "bedrock conductors"), and the apparent resistivity maps better depict broad or flat-lying conductors (Pritchard, 1990). From the paper map, we digitized the locations of bedrock conductors that tracked across at least two adjacent flight lines and plotted them as square spots occurring at flight lines on Figures 5 and 6. The bedrock conductors are omitted from Figure 7 to avoid obscuring the details of the apparent resistivity map. Many of the spots line up to show conductors that continue across many flight lines. Conductance of the digitized anomalies ranged from 1 to more than 100 S (siemens). The variable spacing of the spots is the result of navigation errors, which cause flight lines spacing to vary between 0 and 280 m.

Most of the bedrock conductors coincide with broad areas of low resistivity, but many areas of low resistivity contain no bedrock conductors. In other words, the bedrock conductors appear to have been formed only in broad areas of low resistivity. The bedrock conductors occur in well-defined trends that suggest structural control, and many of them coincide with or are parallel to lineaments, probably faults, identified in air photos (photo lineaments). W.T. Ellis (oral communication, 1998) believes that the bedrock conductors indicate sulfide mineralization formed in fault-controlled vein systems as the culmination of alteration that began as argillic alteration.

Interpretation of Maps of Apparent Resistivity and Bedrock Conductors

The best-defined anomalies, especially at 900 and 7200 Hz, are resistivity highs, shown in blue, usually at higher elevation (e.g. *A-G* in fig. 5; anomaly labels are omitted on figs. 6 and 7 to minimize clutter.). The resistivity highs are interpreted to be caused by erosion-resistant domes and flows having apparent resistivities ranging from 400 to more than 28000 ohm-meters, depending upon the frequency. At 56000 Hz (fig. 7), the resistivity highs are mottled by small areas of lower resistivity probably caused by conductive surficial materials and (or) alteration.

The other set of prominent anomalies is resistivity lows, shown in red (e.g. *J*-*X* in fig. 5), where apparent resistivities range from less than 1 to approximately 70 ohm-meters. Many of the low resistivity zones are at low elevation, but some occur on ridges (e.g. the area between *R* and *L* north of Red Mountain and the area between *P* and *O* south of Orange Mountain). Most of the resistivity lows occur in areas mapped as undifferentiated Popof volcanic rocks (Tpu), although resistivity lows also occur in some areas mapped as dome rocks (Tpdd, Tpdb) and tuff and volcaniclastic rocks (Tpth, Tps). One small area of sedimentary rocks (Tu) coincides with part of a prominent resistivity low (*P*) south of Orange Mountain.

The preceding paragraphs are all we can say with assurance. The four paragraphs that follow represent an attempt to push the interpretive limits of the EM data, and should be viewed only as hypotheses for possible testing in the field.

Many of the bedrock conductors coincide with photo lineaments. One such coincidence occurs along the northeastern part of the Apollo trend (*M*-*U*), and involves magnetic lineament ML2, silicic alteration, and bedrock conductors. Bedrock conductors are absent along the Apollo trend southwest of the Apollo mine, reappearing near the coast. Instead, a discontinuous alignment of bedrock conductors (*M*-*N*-*X*) connects the Apollo trend north of the Apollo mine with the Shumagin trend north of Apollo Mountain. Photo lineaments, bedrock conductors, and two areas of silicic alteration coincide with the Shumagin trend (*Q*-*P*-*O*-*S*), but there is no magnetic lineament. Photo lineaments and bedrock conductors also coincide close to ML3, and others form a southwest-trending zone (*R*-*J*) in the northern part of the geophysical survey. All of these could be considered in the search for mineralization. Note, however, that although isolated bedrock conductors occur close to the Apollo Mine, and a short alignment of bedrock conductors passes near the Shumagin prospect, neither the mine nor the prospect lies on a major trend of conductors, suggesting that typical vein mineralization on Unga Island is not associated with bedrock conductors.

In order to explore the variation of resistivity with depth, we plotted the log of the ratio of apparent resistivity at 7200 Hz to apparent resistivity at 900 Hz (fig. 8). Red and yellow indicate lower resistivity at 900 Hz than at 7200 Hz, hence resistivity decreasing with depth. These areas correlate well with bedrock conductors, and with parts of the Apollo and Shumagin trends. (Ratios involving the 56000 Hz data emphasized northwest trending features that probably reflect mis-leveling of the raw flight line data, and are not included in the final report.)

Approximately 250 m northwest of the Apollo Mine is a resistivity high (at 56000 Hz) 250 m in diameter (fig. 7), and conductivity is higher at depth (resistivity is 6047, 184, and 682 ohm-meters at 56000, 7200, and 900 Hz respectively). (This location does not show as a positive anomaly in Figure 8, because, although resistivity here decreases from 56000 to 7200 Hz, it increases from 7200 Hz to 900 Hz.) Mapped rock types are undifferentiated Popof volcanic rocks (Tpu). Hence the Apollo mine itself is a potential model for a silicified cap overlying a mineralized hydrothermal system. Another area of high apparent resistivity at 56000 Hz, conductivity increasing with depth and bedrock conductors is a 500 m by 1000 m area immediately northeast of the Shumagin prospect (SPr).

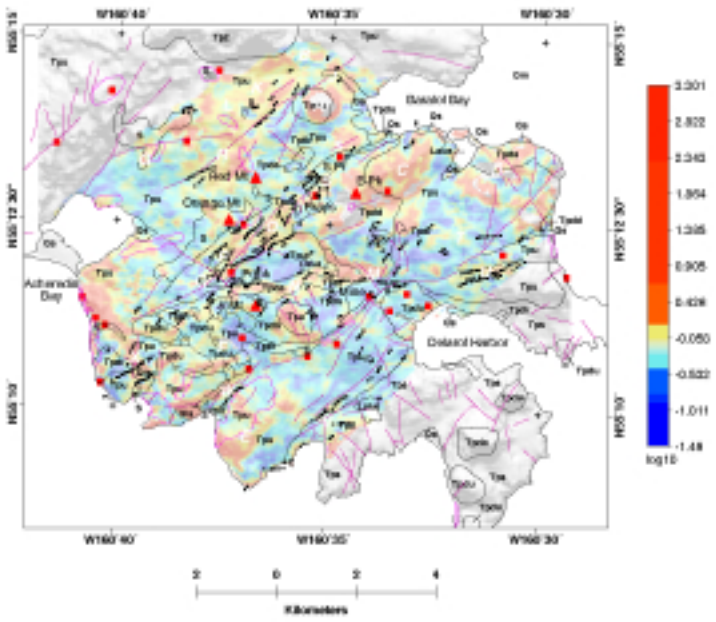

Figure 8

Figure 8. Log of the ratio of apparent resistivity at 7200 Hz to apparent resistivity at 900 Hz. ($\log_{10}((\rho_{a7200Hz}/(\rho_{a900Hz})$. Reds show increasing conductivity with depth. Areas where resistivity at 900 Hz is clipped to 1035 ohm-m, mainly over domes, are colorless. Square black spots indicate "discrete bedrock conductors". Superimposed on topography in shaded relief illuminated from the northeast.

An alternative explanation for conductivity that increases downward is argillic alteration and (or) fluid-filled porosity in tuff. One of the most interesting areas on the resistivity maps is the triangular area of resistivity lows (including *O*, *M*, *N*, *Q*, and *P*) with its apex at Red Mountain and a base that runs just north of Apollo Mountain and the Apollo Mine. This is the area of the Orange Mountain Resistivity Low (OMRL) identified by Ellis and Apel (1991) and attributed to argillic alteration, possibly of tuff. As has been previously discussed, the presence of significant amounts of tuff, altered or otherwise, in the immediate vicinity of Orange Mountain is problematic. Coincident with the northwest side of the triangle (*Q*-*P*-*O*) is a northeast trending zone (identified as Zone 1 by Ellis and Apel, 1991) 700 to 1000 m wide characterized by low resistivity at all frequencies (resistivity 55, 36, and 22 ohm-meters respectively at 56000, 7200, and 900 Hz), conductivity increasing with depth, a strong alignment of bedrock conductors, and photo lineaments. The area is mapped as undifferentiated Popof volcanic rocks (unit Tpu; this publication, Chapter 2). At the southern end of the OMRL is an area of mapped tuff (unit Tpth) coincident with low apparent resistivity and downward-increasing conductivity, which extends from north of Apollo Mountain east to the Apollo mine (this area forms the base of the triangular OMRL, and the eastern two-thirds of the area is labeled *N*-*M* in fig. 8). In this area, the resistivity low is clearly underlain by tuff.

Within the OMRL is a central zone of high resistivity that lies in a critical spot with the following characteristics: 1) ML3 passes through it. 2) It is approximately bounded to the north by coincident bedrock conductors and photo lineaments. 3) It is accompanied by a minor but anomalous east-west trending topographic ridge passing just north of Pook. Geologic field work aimed at deciphering the geology of the central portion of the map area would benefit from a careful look at the resistant bedrock ridge, where bedrock should be more prevalent than elsewhere in this low lying area. 4) It generally lacks bedrock conductors, but it is aligned with a discontinuous band of discrete conductors passing through *M* that suggest a link between the southwestern end of the Shumagin trend and the northeastern end of the Apollo trend. 5) An irregular topographic escarpment, down to the southwest, runs along the northern shore of Baralof Bay through *O* and *M* to *B*, and forms the northeastern boundary of the OMRL. Ellis and Apel (1991) identified a major northwest-trending fault at Orange Mountain as a possible conduit for mineralizing fluids.

Other sites in the area of the geophysical survey having low resistivity at 56000 Hz, downward increasing conductivity, and bedrock conductors, with or without photo lineaments, are: 1) northern apex of the survey, along the trend *R*-*J*, 2) northeastern end of the Shumagin trend (*S*), and 3) northeastern end of the Apollo trend (*U*, which is Zone 2 of Ellis and Apel, 1991). Altered tuff occurs at the east end of the Shumagin lineament, but tuff in significant amounts has not been identified at the other sites by either Riehle and others (Chapter 2) or Ellis and Apel (1991).

To summarize: Broad areas of low resistivity occur in undifferentiated Popof volcanic rocks (unit Tpu), which are dominantly lava flows, as well as over some areas of tuffs. Ellis and Apel (1991) inferred that alteration, especially of tuffs, is the cause of the OMRL. Alternatively, based upon the mapping of Riehle and others (Chapter 2), we suggest that low resistivity is caused by argillic alteration that crosses lithologic boundaries. Locally, alteration could occur preferentially in tuffs, which have high primary porosity, but broadly speaking the alteration is structurally controlled. Such an inference is consistent with Ellis (1992), who refers to structural control of veins and mineral target zones within the OMRL. In support,

we note that some areas of low resistivity contain bedrock conductors that show clear evidence of structural control, such as along the Shumagin and eastern Apollo trends. Aligned conductors also suggest a connection between the Shumagin and Apollo trends, along trend *Q-N-P* (fig. 8). The bedrock conductors may be caused by continuous stringers of massive sulfide and (or) clay in fault gouge. The fact that bedrock conductors are almost exclusively located in broad areas of low resistivity suggest that the conductors form along faults in areas of broad argillic alteration. These speculations cannot be tested without further geologic and geophysical field work.

GEOLOGIC INTERPRETATION OF INTEGRATED AEROMAGNETIC AND ELECTROMAGNETIC DATA

Comparison of the aeromagnetic and resistivity maps reveals some simple correlations between reduced-to-the-pole (RTP) total magnetic intensity and resistivity (fig.9). The most common correlation is that of magnetic highs and resistivity highs caused by domes and flows. Through empirical testing, we classified the map into apparent geologically meaningful regions using threshold values of 52,000 nT for total magnetic intensity and 50 ohm-meters for apparent resistivity. The categories on the map are as shown in the caption to Figure 9.

The map categories correlate fairly well with mapped geologic units. Undifferentiated Popof volcanic rocks (Tpu) are present in all areas, reflecting the variability of rock types lumped into and covered by this mixed unit. Most of the dome rocks occur in the magnetic-resistive category, with the exception of one area of undifferentiated domes (Tpdu) between the Apollo mine and Delarof Harbor. The Apollo Mine and Shumagin prospect occur in the nonmagnetic-resistive areas. The magnetic-conductive and the nonmagnetic-conductive categories contain primarily undifferentiated Popof volcanic rocks (Tpu). These areas tend to coincide with the bedrock conductors in the Shumagin trend and in the eastern part of the Apollo trend. Areas of mapped silicic alteration occur most often in the magnetic-resistive category, and secondly, in the nonmagnetic-resistive category, although some of the silicic alteration in the nonmagnetic-resistive areas lap over into the nonmagnetic-conductive category.

Neither of the authors has been in the field on Unga Island, and no measurements of rock physical properties are available to constrain the interpretations. A geophysicist and exploration geologist should take the geophysical data and preliminary interpretations to the field, preferably using a lap-top computer attached to a GPS system. Relationships between the various data sets can be explored and hypotheses tested in the field. A hand-held magnetic susceptibility meter and portable EM system should be used to determine the magnetic susceptibility and resistivity of characteristic units, and possibly identify bedrock conductors cropping out at the surface.

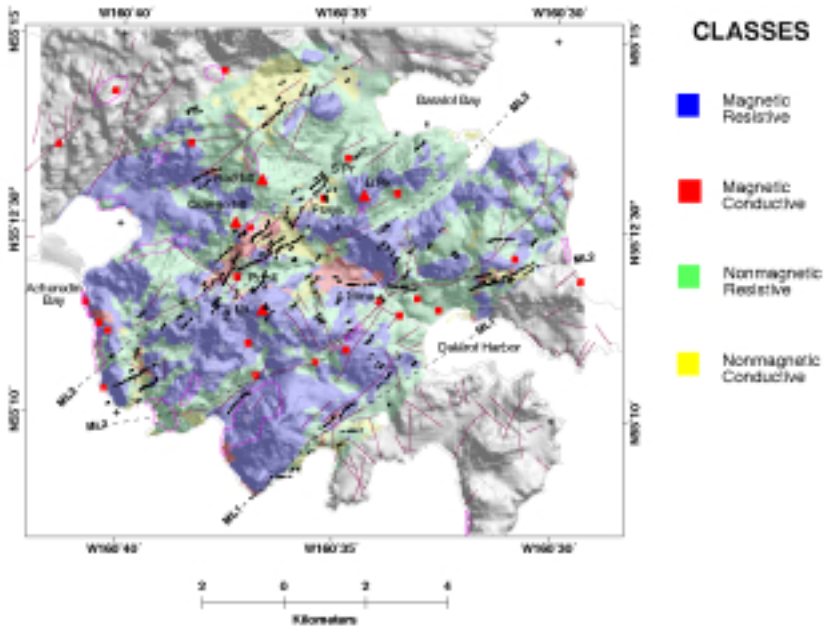

Figure 9. Classification map showing rock physical properties inferred from RTP magnetic data and 7200-Hz resistivity data. Superimposed on topography in shaded relief illuminated from the northeast. Thresholds are 52,000 nT and 50 ohm-m. Square black spots indicate discrete bedrock conductors. Classes are shown below:

Color	Description	Total magnetic intensity (RTP) (nT)	Apparent Resistivity (ohm-m)	Typical Geologic Units	Predicted Rock Types
Blue	Magnetic-Resistive	>52,000	>50	Tpdu, Tpdd, Tpdb, Tpth, Tpu, Tpdr, Tpda	Domes and Flows
Red	Magnetic-Conductive	>52,000	<50	Tpu	Tuff?
Green	Non-mag-Resistive	<52,000	>50	Tpu, Tpdu	Silicified tuff?
Yellow	Non-mag-Conductive	<52,000	<50	Tpu	Argillicly altered tuff?

A good starting point would be to characterize the four classified units of Figure 9. If finding gold mineralization is the goal, the most favorable places to begin would be: 1) Examine the nonmagnetic-resistive (green) areas around the Apollo Mine and Shumagin claims. Look for tuff, and evidence of silicification. Is silicified tuff more resistive and less magnetic than unsilicified tuff? Does silicification occur along the photo lineaments? Is anything different over the rare bedrock conductors in the nonmagnetic-resistive areas? 2) Examine the nonmagnetic-conductive (yellow) areas, especially those containing bedrock conductors and (or) photo lineaments, in the eastern end of the Apollo trend, along the Shumagin trend, and in the northern part of the map west of Baralof Bay. Look for tuff. Does it contain argillic alteration, and is it unsilicified? 3) Are the magnetic-conductive areas tuff? Why are they magnetic? Are discrete conductors exposed at the surface? 4) Look at the boundary between the magnetic-resistive (blue) and nonmagnetic-resistive (green) areas between Red and Orange Mountains (the Orange Mountain resistivity high of Ellis, 1992). Does silicification here correlate with nonmagnetic-resistive rocks?

CONCLUSIONS

Magnetic highs are caused by Tertiary Popof volcanic rocks, especially domes and probably flows. Most of the magnetic sources are exposed at the surface. Typically the magnetic domes, and probably the flows, are more resistant to erosion than the nonmagnetic rocks, such as tuff, and form topographic highs.

Magnetic lineaments ML2 and ML3, defined by discontinuous magnetic lows separating regions of higher magnetic relief, cross Unga Island from southwest to northeast. The lineaments correlate with topographic lows, and are interpreted to indicate the presence of shear zones. However, offset across the lineaments is minor.

Areas of high apparent resistivity correlate with erosion-resistant domes and flows. Areas of low apparent resistivity occur primarily in areas containing argillically-altered Popof volcanic rocks, both lava flows and tuff. Bedrock conductors, probably veins containing pyrite and possibly shear zones containing clay, occur in some, but not all, of the areas of low apparent resistivity. Skin depth at 7200 Hz in the conductive areas is 100 m or less, and the bedrock conductors occur in areas with a skin depth of 50 m or less at 7200 Hz. Therefore, exploration targets associated with conductive rocks should be found at shallow depths.

There is a strong correlation of bedrock conductors with the mineralized Apollo and Shumagin trends, although many of the known deposits lack conductors. Ellis (1992, oral communication 1998) believes that the cause of the conductors is pyrite in vein systems, but we have not conducted fieldwork to confirm this. There is an association of gold geochemical anomalies and low resistivity in the Orange Mountain Resistivity Low that Ellis (1992) suggests may be an indicator of disseminated gold deposits.

ACKNOWLEDGEMENTS

Maryla Dez-Pan and Ric Wilson provided excellent technical reviews that substantially improved the quality of the manuscript.

REFERENCES

Cox, D.P., and Singer, D.A., eds., 1986, Mineral deposit models: U.S. Geological Survey Bulletin 1693, p. 110.

Ellis, W.T., and Apel, Robert A., 1991, Unga/Alaska Peninsula Project, 1990 Final Report: Battle Mountain Exploration Company, Alaska District, 31 p.

Ellis, W.T., 1992, Aleut Corporation Mineral Potential: The Aleut Corporation, Anchorage, Alaska, 22 p.

Fisher, M.A., 1981, Location of the Border Ranges fault southwest of Kodiak Island, Alaska: Geological Society of America Bull., v. 92, p. 19-30.

Gunn, P.J. and Dentith, M.C., 1997, Magnetic responses associated with mineral deposits, AGSO Journal of Australian Geology and Geophysics, v. 17, no. 2, p. 145-158.

Klein, D.P., and Bankey, V., 1992, Geophysical model of Creede, Comstock, Sado, Goldfield and related epithermal precious metal deposits, in Hoover, D.B., Heran, W.D., and Hill, P.L., Editors, The geophysical expression of selected mineral deposit models: U.S. Geological Survey Open-File Report 92-557, p. 98-106.

Moll-Stalcup, E.J., Brew, D.A., and Vallier, T.L., 1994, Latest Cretaceous and Cenozoic magmatic rocks of Alaska, in Plafker, George, and Berg, H.C., eds., The Geology of Alaska: Geological Society of America, The Geology of North America, v. G-1, Plate 5.

Plafker, George, Moore, J.C., and Winkler, G.R., 1994, Geology of the southern Alaska margin, p. 389-449 in Plafker, George, and Berg, H.C., eds., The Geology of Alaska: Geological Society of America, The Geology of North America, v. G-1, p. 389-449.

Pritchard, D.E., 1990, DIGHEM^{IV} Survey for Battle Mountain Exploration Company, Unga and Popof Islands, Alaska, USA: DIGHEM Surveys and Processing Inc., Mississauga, Ontario, 68 p., 3 appendices.

Riehle, J.R., 1999, Geologic structures of Unga Island, their relations to mineralization, and some speculations on their origins: ch. 5 *in* Riehle, J.R., ed., Geological and Geophysical Setting of the Gold-Silver Vein Systems of Unga Island, Southwestern Alaska; U.S. Geological Survey Open-File Report 99-136 (this volume).

Riehle, J.R., Wilson, F.H., Shew, N., and White, W.H., 1999, Geology of Unga Island and the northwestern part of Popof Island, ch. 2 *in* Riehle, J.R., ed., Geological and Geophysical Setting of the Gold-Silver Vein Systems of Unga Island, Southwestern Alaska; U.S. Geological Survey Open-File Report 99-136 (this volume).

Saltus, R.W., and Simmons, G.C., 1997, Composite and merged aeromagnetic data for Alaska: A web site for distribution of gridded data and plot files: U.S. Geological Survey Open-file report 97-520, 14 p.

Saltus, R.W., Hudson, T.L., and Connard, G.G., in press, A new magnetic view of Alaska, submitted to Geology Today.

Singer, D.A., 1999, Classifying the Shumagin and Alaska Apollo deposits, ch. 7 *in* Riehle, J.R., ed., Geological and Geophysical Setting of the Gold-Silver Vein Systems of Unga Island, Southwestern Alaska; U.S. Geological Survey Open-File Report 99-136 (this volume).

Wilson, F.H., Detterman, R.L., Miller, J.W., and Case, J.E., 1995, Geologic map of the Port Moller, Stepovak Bay, and Simeonof Island Quadrangles, Alaska Peninsula, Alaska: U.S. Geological Survey Miscellaneous Investigations Map I-2272, Scale 1:250,000.

Wilson, F.H., White, W.H., Detterman, R.L., and Case, J.E., 1996, Maps showing the resource assessment of the Port Moller, Stepovak Bay, and Simeonof Island Quadrangles, Alaska Peninsula, U.S. Geological Survey Miscellaneous Field Studies Map MF-2155-F, Scale 1:250,000.